

EC135 SYSTEM IDENTIFICATION FOR MODEL FOLLOWING CONTROL AND TURBULENCE MODELING

S. Seher-Weiss and W. von Gruenhagen
DLR Institute of Flight Systems
Lilienthalplatz 7, 38108 Braunschweig, Germany
susanne.seher-weiss@dlr.de, wolfgang.gruenhagen@dlr.de

OVERVIEW

At the DLR Institute of Flight Systems two main purposes are currently driving the system identification activities for the EC135 FHS research helicopter. First, in order to support the in-flight capabilities, models of different complexity are identified that can be used in the development process of the model following flight control system. Second, as part of the US-German memorandum of understanding on helicopter aeromechanics, empirical hover and low-speed turbulence models shall be developed. For the latter, accurate models of the host helicopter have to first be identified from flight tests without turbulence. Both tasks have the need for high fidelity models that are accurate over a broad frequency range. Therefore, the basic 6-DoF rigid body model has been incrementally extended to account for longitudinal and lateral flapping, dynamic inflow, and the rotor lead-lag motion. This resulted in models of increasing complexity of up to 16 states and 11-DoF. The paper describes the model equations used for each of the model extensions and illustrates the resulting improvements both in the time and frequency domain.

1. NOMENCLATURE

a, b	longitudinal and lateral flapping angles
a_x, a_y, a_z	longitudinal, lateral and vertical accelerations
$B\delta_y$	blade root control input
L, M, N	rolling, pitching, and yawing moment derivatives
p, q, r	body axis roll, pitch, and yaw rates
s	Laplace variable
T	thrust (aerodynamics only) derivative
u, v, w	longitudinal, lateral, and vertical velocities
x, y	internal states for lead-lag modeling
X, Y, Z	longitudinal, lateral, and vertical force derivatives
δ_x, δ_y	longitudinal and lateral cyclic input
δ_0, δ_p	collective and pedal input
Φ, Θ	roll and pitch angles
ζ, ω	damping and natural frequency of a complex eigenvalue
τ	time constant
v	inflow

2. INTRODUCTION

Accurate and flight test validated models of the EC135 helicopter are needed both for the development of the model following flight control system and as a basis for the development of controller equivalent turbulence models. Thus system identification has to be performed in order to arrive at high fidelity models that include rotor effects. Depending on the application of the models, they have to be valid over different frequency ranges. Therefore, different levels of complexity are needed and time domain as well as frequency domain methods have to be applied.

2.1. EC135 Flying Helicopter Simulator

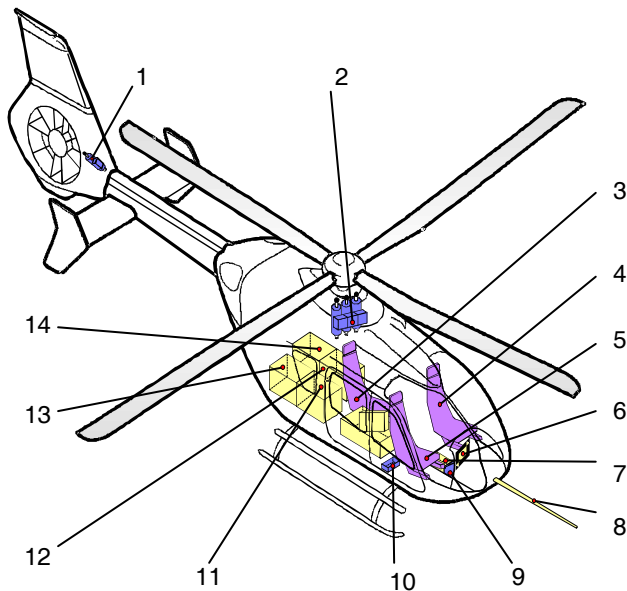
The basic aircraft for the flying helicopter simulator¹ (FHS) is a Eurocopter EC135 helicopter (Figure 1). It is a modern, twin-engine, light helicopter with a bearingless main rotor and fan-in-fin tail rotor. It is evident that an in-flight simulator cannot represent an aircraft with faster dynamic responses than those of the basic aircraft. Therefore, a fundamental requirement for airborne simulation is a high dynamic response capability of the basic vehicle. The EC135 is a rotorcraft with very high agility particularly due to its main rotor system with an equivalent hinge offset of 8.7%. That allows a roll bandwidth of about 3.7 rad/s and a pitch bandwidth of approximately 1.8 rad/s (see²).



FIG 1. The Flying Helicopter Simulator EC135 (FHS)

The basic EC135 is equipped with a conventional mechanical control system with hydraulic boosters. The FHS user requirements clearly indicated that the mechanical system had to be replaced by a full authority digital flight control system using fly-by-wire and fly-by-light technology. A hierarchical system architecture was defined to meet the two major requirements of safety and flexibility. The PFCS (primary flight control system) meets civil certification requirements with a probability of catastrophic failures of less than 10^{-9} per flight hour and thus provides the safety.

Flexibility is provided by the “experimental system” with the experimental computer and the data management computer. The experimental computer communicates with the core system computer. It receives the evaluation pilot command signals, modifies them according to the programmed control laws and transfers them back to the core system. The data management computer collects all data provided by basic sensors as well as sensors in the experimental system, and transfers them to the telemetry, the on-board data recording, and to the graphics computer that controls the displays.



- 1 Tail Rotor Actuator
- 2 Main Rotor Actuators
- 3 Flight Test Engineer
 - Display, Quicklook
 - Experimental System, Control & Display Unit
- 4 Safety Pilot
- 5 Experimental Pilot
- 6 Experimental Pilot Display
- 7 Experimental System Control & Display Unit
- 8 Air Data Sensor
- 9 Core System Computer
- 10 Control Signal Processing Computer
- 11 Simulation Computer
- 12 Data Management, Telemetry, Data Recording
- 13 Additional Equipment
- 14 Graphics Computer, Rotor Data Acquisition

FIG 2. FHS System Architecture

Figure 2 illustrates the technical realization of the architecture and some of the major helicopter modifications. The EC135 cabin accommodates a three men crew with a safety pilot on the left pilot seat and an evaluation pilot on the right pilot seat. A flight test engineer station is located behind the two pilots. Both pilots have conventional controls (stick, collective, pedals). The original mechanical control system was replaced by flexball cables, which connect the safety pilot controls with the hydraulic actuators as a mechanical back-up.

As a research helicopter, the FHS is fully instrumented with a number of redundant sensors and measuring equipment. The instrumentation system mainly includes two air data units (static and differential pressure, temperature, altitude, airspeed), two AHRS (attitude and heading reference systems), a radar altimeter, FADEC (full authority digital engine control) data, individual linear accelerometers, INS (inertial navigation system), nose boom air data (static and dynamic pressure, angle of attack and sideslip, temperature), differential GPS, and control input signals at various positions.

2.2. Model Following Control System

In the whole development process of FHS in-flight simulation three research disciplines play a major role, i.e. non-linear modeling of helicopter dynamics, helicopter system identification and control system design³. All three of them are tightly entwined with each other and based on a detailed system analysis (see figure 3).

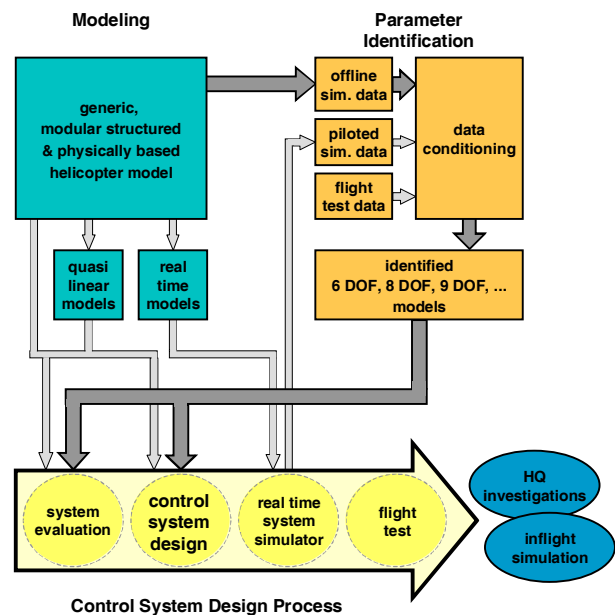


FIG 3. Control System Development

It is obvious that in order to reduce the costs arising from flight tests for adjusting and tuning control system parameters, a highly accurate helicopter model suitable for pilot and hardware in-the-loop testing is indispensable. Especially, the simulation model bandwidth and coupling behavior has to correspond with the controller bandwidth for a correct design of the latter.

The paper will describe in detail model extensions for flapping, dynamic inflow, and rotor lead-lag that were incorporated in order to improve the helicopter cross-coupling prediction capabilities.

As can be seen from figure 3, identification is performed using flight test data, piloted simulation data as well as off-line simulation data. The identified models from off-line simulated data found application in the beginning of the control system design process, since they easily allowed for parameter and configuration studies (e.g. stability margin estimation). However, in the final design for the flying system, models identified from FHS flight test data are used. In this paper only results of the system identification from flight test data will be shown.

Industry partners will use the FHS mostly as a technology demonstrator, whereas for DLR the active control technology is the most interesting aspect. Here, the applications will vary from open loop techniques such as passive (e.g. gains) and active control (e.g. time dependant elements filters and delays) mixing of the pilot commands to the more demanding closed loop applications, in particular the model following control (MFCS) approach. The typical structure of the MFCS is shown in figure 4.

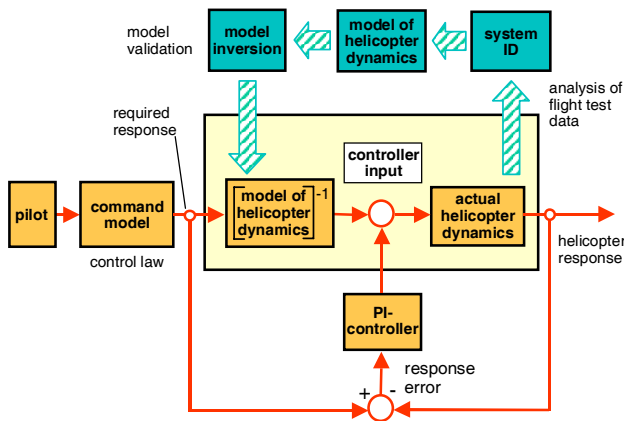


FIG 4. MFCS Principal Structure

The MFCS approach is used to investigate advanced controller systems, variations of basic handling qualities and to simulate other helicopters in flight.

All active control applications make use of identified models. For open loop applications 6-DoF models will normally be sufficient, whereas the MFCS application requires higher order 8- to 11-DoF models. Currently, the command model uses the identified 8-DoF model. The inverse model of the helicopter used in the feed forward branch is a 9-DoF model that is based on the identified 11-DoF model but neglects the rotor lead-lag.

3. CONTROLLER EQUIVALENT TURBULENCE INPUT MODELS

For helicopters, precision hover tasks in adverse weather are an important mission but the most difficult to model. Reliable flight test validated hover turbulence models are needed.

The traditional approach to turbulence modeling for fixed wing aircraft is the use of a frozen gust pattern, most commonly generated from a Dryden spectral model. For frozen gust patterns, the reaction of the aircraft to the turbulence is a function of the relative velocity with respect to the air mass through which it is flying. They are therefore not applicable for hovering helicopters because the relative velocity goes to zero. Even though frozen gust patterns generated from Dryden turbulence models have received favorable comments at high speed forward flight, helicopter pilots have criticized them as not being representative for low speed flight⁴.

Therefore, an alternative approach for the extraction of turbulence models has been developed by Lusardi⁵ (see figure 5). Data is collected from flight in heavy turbulence, such as for example generated from flight on the leeward side of a large building in strong winds. The measured aircraft responses are fed into an inverse aircraft model to obtain control inputs related to pilot and gusts. Subtracting the measured pilot inputs yields equivalent control input traces that correspond to the response of the aircraft to the gusts. In order to keep the pilot inputs mostly uncorrelated from the turbulence itself, the pilot is instructed to just roughly hold the position without correcting all disturbances caused by turbulence.

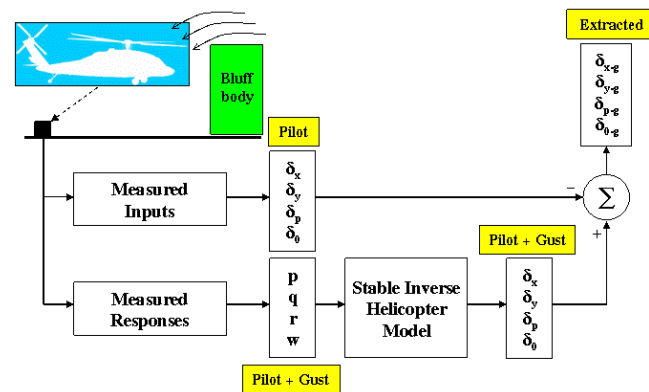


FIG 5. Gust Extraction by Inverse Modeling

The extracted control disturbances are used to develop white noise driven transfer functions of a form similar to Dryden models. The aim is to arrive at a general turbulence model that is scalable with wind speed and turbulence intensity and can be used for control system and flying qualities investigations. The technique has successfully been demonstrated with the UH-60 helicopter.

Buchholz⁶ suggests a different approach for extraction of the equivalent control inputs (see figure 6). It does not need an inverse model of the aircraft, but instead an observer approach is used. The pilot inputs measured under turbulent conditions are fed into a nominal model of the aircraft to obtain the aircraft response caused by the pilot inputs. This calculated response is subtracted from the measured response (including gusts) and the error is fed back and added to the pilot inputs. The fed back controls are then also related to the response of the aircraft due to the gusts.

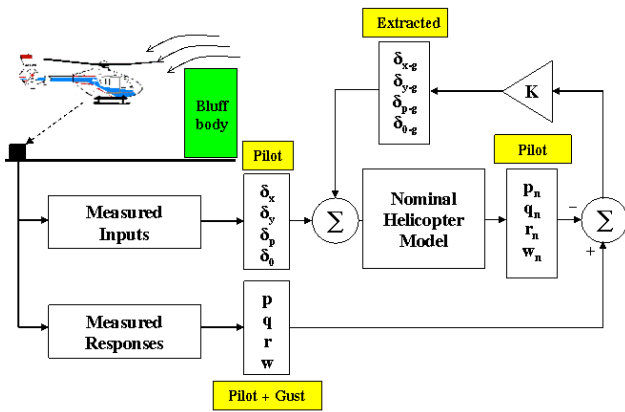


FIG 6. Gust Extraction by Observer

Both approaches for gust extraction need accurate models of the aircraft. So far, a model for the hover condition which accounts for flapping and dynamic inflow but neglects the longitudinal axis (a_x, u) has been identified. Rotor lead-lag is not yet included because the EC135 has a lead-lag damper which makes this effect less pronounced than for example for a BO105 with its hingeless rotor system. Should the evaluation of the flight tests which are planned but have not yet been flown, show that the lead-lag motion has to be accounted for, the model has to be extended accordingly.

4. MODELING

The quasi-steady formulation of the helicopter dynamics by a classical 6-DoF rigid body model is valid only up to about 10 rad/s. To arrive at high fidelity models that are valid up to 30 rad/s, as is required for model following control, the higher order effects of rotor flapping, dynamic inflow, and rotor-lead-lag have to be accounted for. As the identified models have to be invertible, only linear models can be used.

4.1. Flapping

To account for flapping, the first order on-axis response for the roll rate

$$(1) \dot{p} = L_p p + L_{\delta_y} \delta_y$$

is replaced by

$$(2) \begin{aligned} \dot{p} &= L_b b \\ \dot{b} &= -p - 1/\tau_b b + B_{\delta_y} / \tau_b \delta_y \end{aligned}$$

where b is the lateral flapping angle. The first equation from (2) makes the roll acceleration proportional to the lateral flapping angle. The second equation is a first order rotor equation with τ_b as the lateral flapping time constant. Similar equations hold for the longitudinal flapping coupled to pitch rate.

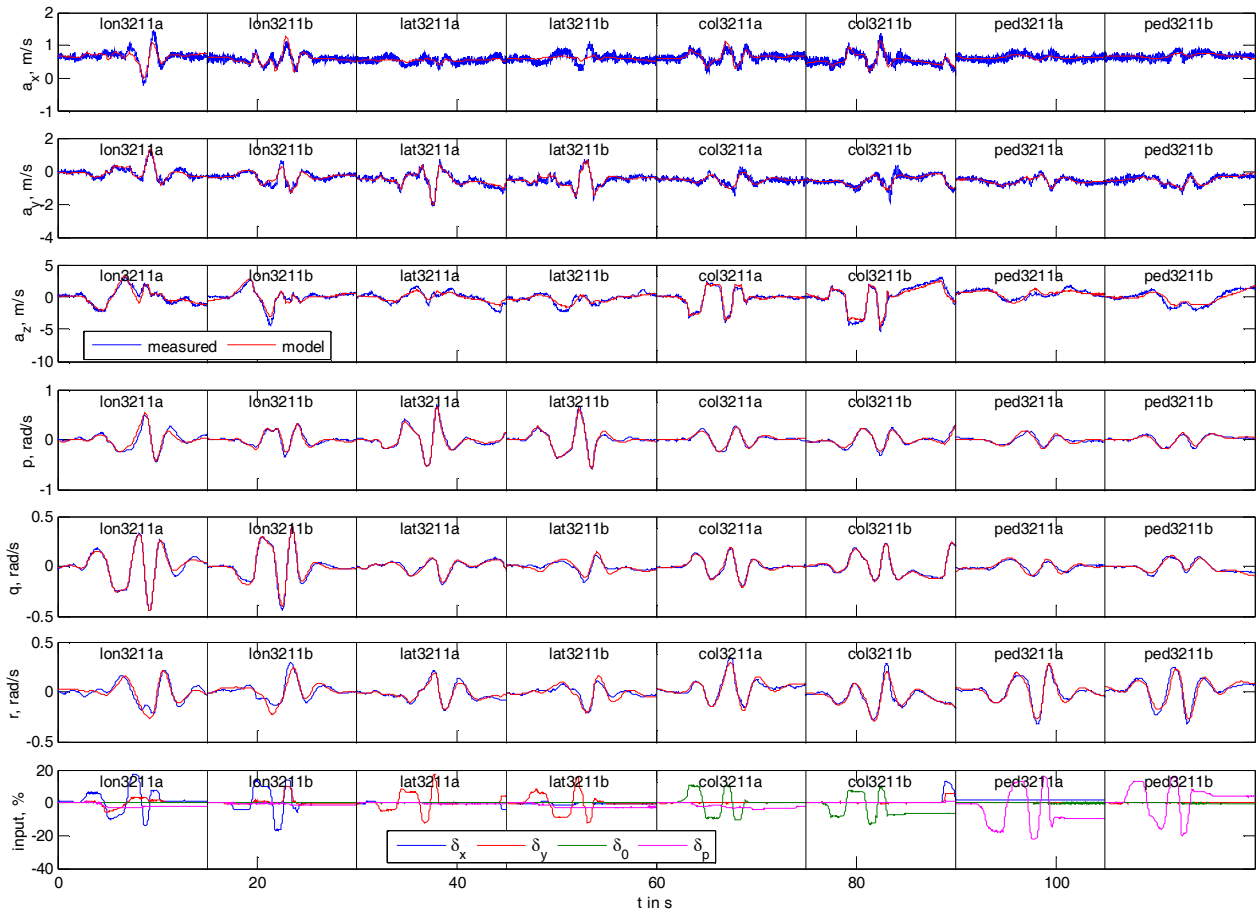


FIG 7. Time Domain Match of the Identified 8-DoF Model for 60 kts Forward Flight

Using this type of equation for the flapping is not optimal for system identification as the flapping angles are usually not measured and thus not available as output variables to be matched. The model is therefore reformulated by differentiating the first equation from (2) and inserting the second as well as the equation for b from (2a), which results in

$$(3) \quad \begin{aligned} \ddot{p} &= -L_b p - 1/\tau_b \dot{p} + L_b B \delta_y / \tau_b \delta_y \\ &= \hat{L}_p p + \hat{L}_p \dot{p} + \hat{L}_{\delta_y} \delta_y \end{aligned}$$

The corresponding equation for pitch rate is

$$(4) \quad \ddot{q} = \hat{M}_q q + \hat{M}_q \dot{q} + \hat{M}_{\delta_x} \delta_x$$

The incorporation of the flapping motion using this model thus leads to \dot{p} and \dot{q} as two additional state variables, resulting in an 8-DoF model with 10 states.

Figure 7 shows the time domain match for the 8-DoF model that was identified for the 60 kts forward flight condition. It can be seen that the on-axis as well as the off-axis responses are predicted quite well. This identified model is used as the basis for the command model in the model following flight control system (see figure 4). For this application, the emphasis is more on the steady-state and less on the short-term response. Therefore, a time domain identification method was applied. The data evaluated consisted of pilot generated 3211 multistep maneuvers in all controls.

4.2. Dynamic Inflow

The dynamic equations for vertical velocity w and inflow v for a rigid rotor (neglecting coning) are

$$(5) \quad \begin{aligned} \dot{w} &= Z_w w + Z_v \dot{v} + Z_v v \\ \dot{v} &= T_w w + T_v v + T_{\delta_0} \delta_0 \end{aligned}$$

Here, the thrust equation (5b) is derived from the principle of linear momentum. Inserting the second equation from (5) into the first eliminates \dot{v} and leads to

$$(6) \quad \begin{aligned} \dot{w} &= (Z_w + Z_v T_w) w + (Z_v T_v + Z_v) v + Z_v T_{\delta_0} \delta_0 \\ &= \bar{Z}_w w + \bar{Z}_v v + \bar{Z}_{\delta_0} \delta_0 \end{aligned}$$

Solving for v yields

$$(7) \quad v = 1/\bar{Z}_v (\dot{w} - \bar{Z}_w w - \bar{Z}_{\delta_0} \delta_0)$$

Differentiating equation (6) with respect to time and inserting the expressions for \dot{v} and v from (5) and (7) gives

$$(8) \quad \begin{aligned} \ddot{w} &= (\bar{Z}_v T_w - T_v \bar{Z}_w) w + (\bar{Z}_w + T_v) \dot{w} \\ &\quad + (\bar{Z}_v T_{\delta_0} - T_v \bar{Z}_{\delta_0}) \delta_0 + \bar{Z}_{\delta_0} \dot{\delta}_0 \\ &= \hat{Z}_w w + \hat{Z}_{\dot{w}} \dot{w} + \hat{Z}_{\delta_0} \delta_0 + \hat{Z}_{\dot{\delta}_0} \dot{\delta}_0 \end{aligned}$$

This differential equation for \ddot{w} has both δ_0 and $\dot{\delta}_0$ as inputs. Alternatively, $\dot{\delta}_0$ can be added to the model as a

state variable, which then leaves $\dot{\delta}_0$ as the only vertical control input.

This approach is equivalent to the one suggested by Schoeder et. al.⁷ where the dynamic inflow is approximated by a first-order lead-lag filter on the collective term in the vertical axis.

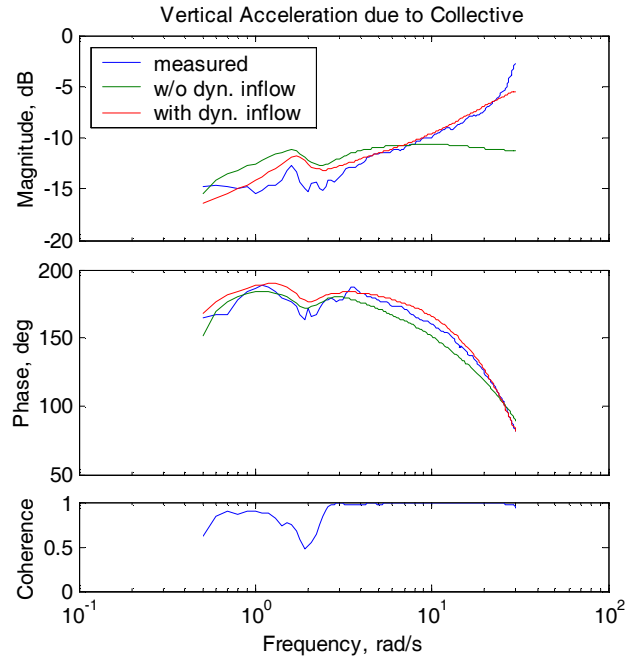


FIG 8. Frequency Domain Comparison for Vertical Acceleration due to Collective Input

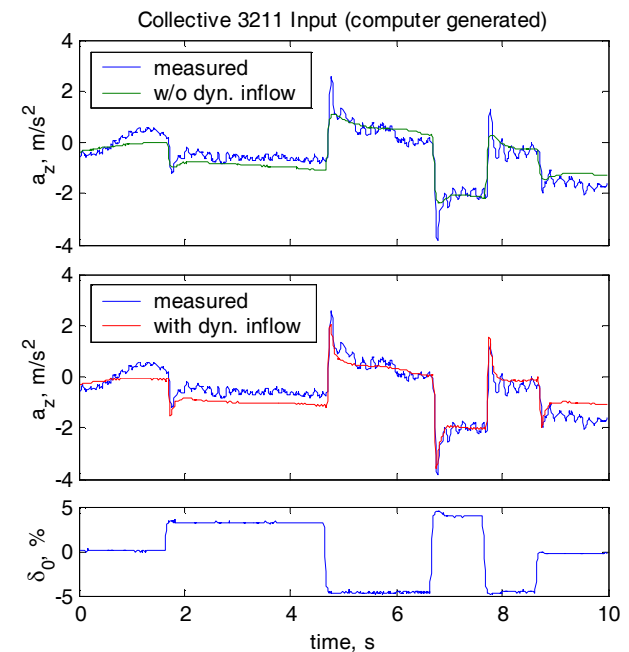


FIG 9. Time Domain Comparison for Vertical Acceleration due to Collective Input

Figure 8 shows that modeling of the dynamic inflow is necessary to capture the rising amplitude in the frequency

response for vertical acceleration due to collective input. Also the match in phase angle is better for the model with dynamic inflow. The slight drop in coherence around 2 rad/s is due to cross-coupling with the dutch roll motion.

Figure 9 compares the time responses of the identified models with and without dynamic inflow. It can clearly be seen, that the model without dynamic inflow does not capture the initial overshoots in the vertical acceleration. The maneuver used for this simulation is a computer generated 3211 multistep collective input.

4.3. Lead-Lag

Simple physical models for the lead-lag dynamics, such as those for the flapping dynamics, are not available. Therefore, a modal approach is usually taken, where a second order dipole is appended to the pitch and roll rate responses due to longitudinal and lateral input⁸.

$$(9) \quad \left(\frac{q}{\delta_x} \right)_{11Dof} = \left(\frac{q}{\delta_x} \right)_{9Dof} \frac{[\zeta_{xq}, \omega_{xq}]}{[\zeta_{ll}, \omega_{ll}]}$$

Here, $[\zeta, \omega]$ denotes a complex zero with damping ζ and natural frequency ω and the index ll stands for lead-lag mode. Four of these dipoles ($\delta_x \rightarrow q$, $\delta_x \rightarrow p$, $\delta_y \rightarrow p$, $\delta_y \rightarrow q$) and a common denominator are necessary.

The transfer functions of these lead-lag dipoles are formulated to have a low order coefficient of 1 such that the low-frequency part of the transfer function (derived from the model without lead-lag) is left unchanged when the dipole is added. Regarding the pitch rate due to longitudinal cyclic input $\delta_x \rightarrow q$, the transfer function thus is

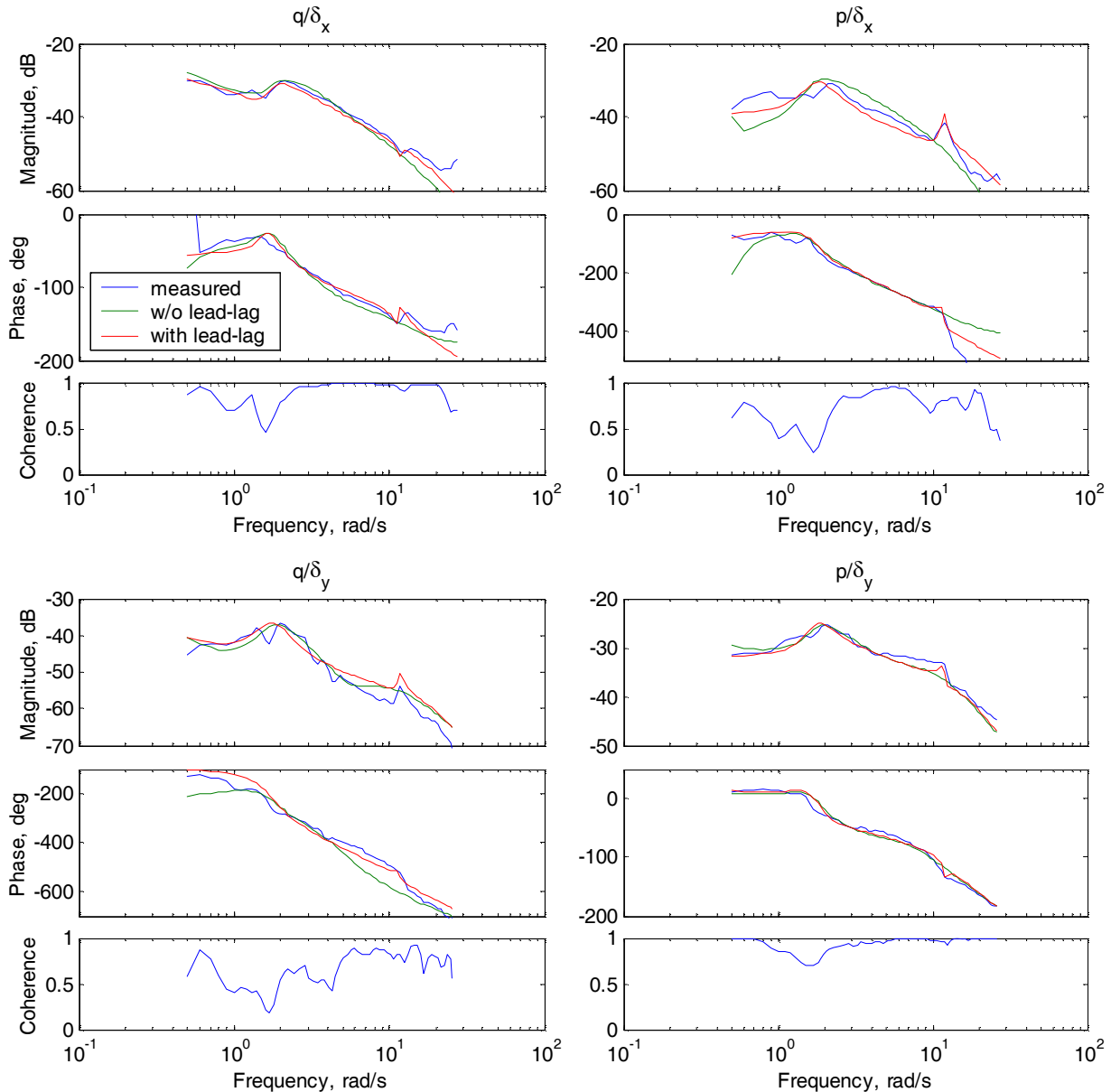


FIG 10. Frequency Domain Comparison of Pitch and Roll Rate due to Longitudinal and Lateral Cyclic Input

$$(10) \quad \frac{\delta_{xq}}{\delta_x} = \frac{(s^2 + 2\zeta_{xq}\omega_{xq}s + \omega_{xq}^2) / \omega_{xq}^2}{(s^2 + 2\zeta_{ll}\omega_{ll}s + \omega_{ll}^2) / \omega_{ll}^2}$$

$$= \frac{\omega_{ll}^2}{\omega_{xq}^2} \left(1 + \frac{2(\zeta_{xq}\omega_{xq} - \zeta_{ll}\omega_{ll})s + (\omega_{xq}^2 - \omega_{ll}^2)}{s^2 + 2\zeta_{ll}\omega_{ll}s + \omega_{ll}^2} \right)$$

For use in a state space identification model, the transfer functions of the dipole have to be transformed into differential equations. We introduce an instrumental variable x that is defined by

$$(11) \quad \frac{x}{\delta_x} = s^2 + 2\zeta_{ll}\omega_{ll}s + \omega_{ll}^2$$

and thus has the differential equation

$$(12) \quad \ddot{x} + 2\zeta_{ll}\omega_{ll}\dot{x} + \omega_{ll}^2x = \delta_x$$

This second order differential equation is transformed into two first order differential equations by introducing $x_1 = x$ and $x_2 = \dot{x}$

$$(13) \quad \begin{aligned} \dot{x}_1 &= x_2 \\ \dot{x}_2 &= -\omega_{ll}^2x_1 - 2\zeta_{ll}\omega_{ll}x_2 + \delta_x \end{aligned}$$

The output equation for δ_{xq} can be derived from (10), as

$$(14) \quad \begin{aligned} \delta_{xq} &= \frac{\omega_{ll}^2}{\omega_{xq}^2} (\omega_{xq}^2 - \omega_{ll}^2)x_1 \\ &+ 2\frac{\omega_{ll}^2}{\omega_{xq}^2} (\zeta_{xq}\omega_{xq} - \zeta_{ll}\omega_{ll})x_2 + \frac{\omega_{ll}^2}{\omega_{xq}^2} \delta_x \end{aligned}$$

This last equation describes how the original control input δ_x is to be replaced in the differential equation for \dot{q} . Equation (14) contains two terms that are to become part of the system matrix and one that belongs to the control matrix.

Regarding the structure of the dipole listed in (10), it can be seen that two differential equations of the form (13) are needed for each control input (δ_x, δ_y). The coefficients in these two pairs of first order differential equations are the same for both controls, as all dipoles share the same denominator.

When the 8-DoF model including flapping is augmented both with the model for dynamic inflow from the previous section and the differential equations for the lead-lag dipoles, the resulting model is an 11-DoF model with 16 states.

Figure 10 shows the improvement in the on- and off-axis frequency response match for pitch and roll rate due to longitudinal and lateral cyclic input when lead-lag modeling is added. Table 1 lists the identified values for the lead-lag parameters.

	ζ	ω
Lead-lag	+0.037	11.67
$\delta_x \rightarrow q$	-0.031	10.97
$\delta_x \rightarrow p$	+0.032	11.93
$\delta_y \rightarrow p$	+0.055	11.87
$\delta_y \rightarrow q$	+0.027	12.08

TAB 1. Identified Lead-Lag Parameters

It can be seen that rotor lead-lag is an effect that is very localized in frequency (around 12 rad/s). Thus it is important to have good starting values in order for the overall model to converge. Starting values for the lead-lag dipoles were determined by first approximating the corresponding transfer functions by simple polynomial models. The dipoles identified from this transfer function fitting were then used as starting values in the identification of the state space model.

Figure 11 shows the improvement in the time domain match once the lead-lag effect is included. The oscillation in the roll acceleration following the second sharp input of the 3211 multistep signal can now be matched. The fit in the main peaks is unchanged, indicating that the lead-lag motion is decoupled from the flapping.

This effect was already recognized in the identification process of the BO 105 helicopter with its hingeless rotor system⁹. It is less distinct here, as the EC135 has mechanical (elastomeric) lead-lag dampers with a nonlinear damping behavior. The right part of figure 11 is an enlarged view of the areas marked by dashed lines in the plot of the whole maneuver as shown on the left, to make the effect more visible.

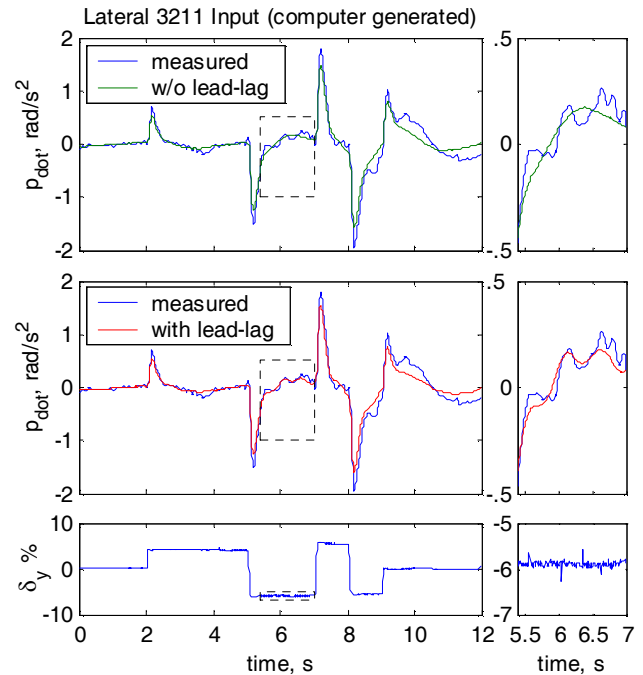


FIG 11. Time Domain Comparison for Roll Acceleration due to Lateral Cyclic Input

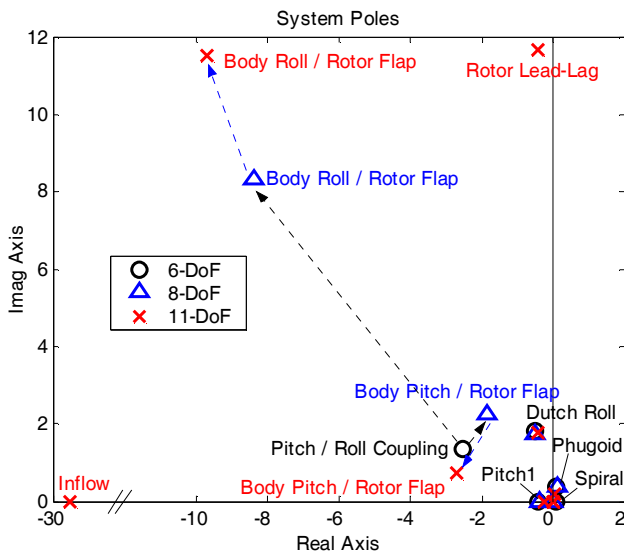


FIG 12. Poles of the Identified Systems

The poles of the identified 6-, 8-, and 11-DoF models for the 60 kts flight condition are compared in figure 12 and the corresponding eigenvalues are listed in table 2. All three models have an unstable spiral and a slightly unstable phugoid. The Dutch roll is virtually the same for all models and all models show a real negative pitch damping eigenvalue. For the 6-DoF model, the two additional real eigenvalues for pitch and roll damping, that are normally present, have joined to form a complex eigenvalue named pitch/roll coupling in the figure.

	6-DoF	8-DoF	11-DoF
Spiral	(-0.065)	(-0.008)	(-0.009)
Phugoid	[-0.23, 0.37]	[-0.29, 0.38]	[-0.24, 0.18]
Pitch1	(0.40)	(0.38)	(0.27)
Dutch Roll	[0.26, 1.86]	[0.28, 1.80]	[0.24, 1.81]
Pitch / Roll Coupling	[0.88, 2.87]	—	—
Body Pitch / Rotor Flap	—	[0.64, 2.92]	[0.97, 2.80]
Body Roll / Rotor Flap	—	[0.71, 11.8]	[0.64, 15.0]
Lead-Lag	—	—	[0.037, 11.7]
Inflow	—	—	(29.5)

TAB 2. Identified System Poles

$$[\zeta, \omega] \text{ implies } s^2 + 2\zeta\omega s + \omega^2 \text{ and}$$

$$(1/T) \text{ implies } s + 1/T$$

Once flapping is included in the 8-DoF model, this pitch/roll coupling eigenvalue separates into two complex eigenvalues. One is due to the coupling of lateral rotor flapping couples with the body rolling motion and the other due to body pitching motion coupled with the longitudinal rotor flapping.

Including dynamic inflow and rotor lead-lag in the 11-DoF model adds a complex high frequency lead-lag pole that is only lightly damped as well as an additional real pole for the inflow. The coupling of the rotor flapping with the body rolling and pitching motion remains but the eigenvalues move towards higher damping (body roll / rotor flap) resp. higher frequency (body pitch / rotor flap).

The feed-forward model of the model following flight control system is based on the identified 11-DoF model. The lead-lag dipoles are discarded for the development of the control system, but they have to be included in the identification model in order to identify the time delays correctly.

The identification of 11-DoF models has been performed both for 60 kts forward flight and hover. For the forward flight condition, the controller based on the identified model has already been flight tested. Development of the corresponding control system for hover is currently under way.

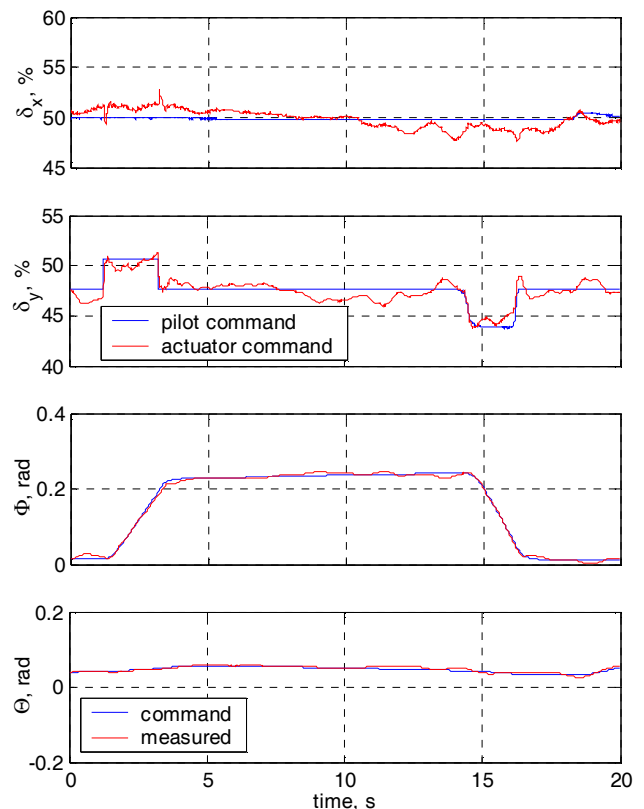


FIG 13. Example: Rate Command Attitude Hold

Figure 13 shows a performance example of the model following quality in forward flight gathered during flight testing of the control system in 'rate command attitude hold' mode.

The model to be followed here is a decoupled modified EC135 model. To perform a turn the pilot has to give a ramp input, he stops the input when the desired bank angle is reached. The hold function is achieved by appropriate feedback gains. The overall controller activity can be seen from the red curves in the two top subplots.

5. SUMMARY

System identification for the EC135 has been performed for 60 kts forward flight as well as for the hover condition. The complexity of the models ranges from 6-DoF rigid body models to 16 state 11-DoF models that include flapping, dynamic inflow and rotor lead-lag.

The identified models are going to be used as a basis for the development of the model following flight control system as well as for the development of controller equivalent turbulence models.

For the model following flight control system, flight tests with controllers based on the identified models for the forward flight condition have already been performed. For hover, the refinement of the control system is ongoing.

A hover model including flapping and dynamic inflow but neglecting the motion in longitudinal direction has been identified and shall form the basis for the development of the turbulence models. The quality of this model can only be assessed once the corresponding flight tests in turbulence are available and the techniques being described will be applied.

6. REFERENCES

- [1] J. Kaletka, H. Kurscheid, U. Butter: *FHS, the New Research Helicopter: Ready for Service*, 29th European Rotorcraft Forum, Friedrichshafen, Germany, Sep. 2003
- [2] K. Kampa, B. Enenkl, G. Polz, G. Roth: *Aeromechanic Aspects in the Design of the EC135*. 23rd European Rotorcraft Forum, Dresden, Germany, Sep. 1997.
- [3] M. Hamers, W. von Gruenhagen: *Advanced Modelling Approach for ACT/FHS Controller Development*, 27th European Rotorcraft Forum, Moscow, Russia, Sep. 2001.
- [4] R.E. McFarland, K. Duisenberg: *Simulation of Rotor Blade Element Turbulence*, NASA Technical Memorandum 108862, Jan. 1995.
- [5] J. Lusardi: *Control Equivalent Turbulence Input Model for the UH-60 Helicopter*. Dissertation, UC Davis, Jun. 2004.
- [6] J. J. Buchholz, W. von Gruenhagen: *Inversion Impossible?*, DLR Institute Report IB 111-2003/34, Dec. 2003.
- [7] J. Schroeder, M. B. Tischler, D. C. Watson and M. M. Eshow: *Identification and Simulation of a Combat Helicopter in Hover*. Journal of Guidance, Control, and Dynamics, Vol. 18, No. 1, Jan-Feb 1995.
- [8] M. B. Tischler, M. G. Caufmann: *Frequency Response Method for Rotorcraft System Identification: Flight Applications to BO 105 Coupled Rotor/Fuselage Dynamics*. AHS Journal, Vol. 37, No. 4, Jul. 1992.
- [9] J. Kaletka, M. B. Tischler, W. von Gruenhagen, J. W. Fletscher: *Time and Frequency Domain Identification and Verification of BO 105 Dynamic Models*. 15th European Rotorcraft Forum, Amsterdam, The Netherlands, Sep. 1989.